Wind turbine drive train vibration with focus on gear dynamics under nondeterministic loads

Citation for the original published paper (version of record):

Struggl, S., Berbyuk, V., Johansson, H. (2012). Wind turbine drive train vibration with focus on gear dynamics under nondeterministic loads. Proceedings, International Conference on Noise and Vibration Engineering, ISMA2012; International Conference on Uncertainty in Structural Dynamics, USD2012. Editors : P. Sas, D. Moens, S. Jonckheere. KU Leuven (Belgium), 17 - 19 September 2012: 4421-4434

ISMA 2012

USD 2012

Proceedings

International Conference on Noise and Vibration Engineering

International Conference on Uncertainty in Structural Dynamics

How to use this CD-Rom

About the conference

Table of Contents

Book of Abstracts

Author Index

KU Leuven (Belgium), 17 - 19 September 2012

Editors : P. Sas, D. Moens, S. Jonckheere

KU LEUVEN

D/2012/5789/1
ISBN 9789073802896

Wind turbine drive train vibration with focus on gear dynamics under nondeterministic loads

S. Struggl, V. Berbyuk, H. Johansson
Chalmers University of Technology, Applied mechanics,
SE 41296, Göteborg, Sweden
e-mail: **stephan.struggl@chalmers.se**

Abstract
In present-day, the engineering challenge around a drive train design for a wind turbine is not only to enhance system reliability but also to reduce the turbine top mass. These requirements together with the trend of upscaling affect many system characteristics and parameters. The proposed contribution presents a model to study torsional drive train vibration dynamics of a generic indirect drive multi-MW wind turbine. The main focus lies on developing a fully parameterized computational model of a multi-stage gearbox which fulfills the requirement of a proper gear dynamic representation appropriate for multibody formalism as well as the requirement to be computationally efficient. Two different strategies for modeling the gear contact are studied and compared in time domain. An analysis of a multi-stage gearbox together with a generator load and a turbine specific nondeterministic excitation was carried out. It is believed that the obtained results will help designer to improve drive train components and to enhance wind turbine reliability and cost efficiency.

1 Introduction

To have a better understanding of wind turbine dynamics, several institutions devoted their efforts on developing simulation tools capable of predicting complete wind turbine behavior under different loading conditions, see [1]. These tools are mostly used for certification, structural analysis and system performance investigations. In today´s wind turbine simulation codes, computational efficiency has been emphasized in order to study a large number of different design load cases as stated in standard 61400-1. These aeroelastic codes are used to model wind turbine behavior during normal and fault conditions by applying the most relevant loads e.g. gravitational loads, inertial loads and operational loads consisting of generator torque and loads produced by control e.g. during start-up, shut- down and yawing. Less effort has been put on modeling the gearbox and its internal dynamics. Nowadays, there is a need for more comprehensive drive train models including a gearbox avoiding oversimplification e.g. by just assuming a gearbox ratio. The trend in wind power technology development has emphasized the gearbox as one of the most crucial components in any reliability assessment of a wind turbine, see [2, 3]. Generally, gear meshing is a complex mechanical interaction due to e.g. contact mechanics, moving multiple contact points along the line of action, backlash, an eventual contact loss during tooth separation close to resonances, time varying mesh stiffness and mesh damping, compliances and damping of shafts, bearings and gearbox housing, misalignments, moreover, specifically for planetary gear the load sharing behavior of the planets. Hence, a large number of research work can be found in the literature contributing to those phenomena by using different approaches e.g. finite element formalism, analytical lumped parameter approach or multibody approaches potentially including flexibilities for certain parts. A comprehensive overview of different mathematical gear models can be found in [4] and later on in [5]. Another issue is to find approaches which can deal with modeling on different scales dealing with complete system dynamics on macro scale as well as on micro scale e.g. including contact phenomena.

A work which overcomes this difficulties by connecting a multibody formalism with an external program specialized in gear meshing analysis by an user- defined force element is presented in [6]. An analysis dedicated to wind turbine drive train dynamics by using multibody models with different levels of complexity i.e. torsional (1 DOF), rigid multibody (6 DOF) and flexible multibody modeling is presented in [7]. Investigations contributing to torsional modeling can be found in reference [8] by introducing a time- dependent pressure angle and contact ratio. The authors in [9, 10] focus on modal properties and torsional oscillations. One can notice that still different levels of complexity are necessary depending on the type of investigation regarding wind turbine drive train systems.
In the present paper the authors propose a torsional multibody model for a drive train system of a wind turbine. The gear contact forces are computed using two different approaches denoted below as "Contact Force Adams" and "Contact Force Subroutine". These are compared and investigated taking backlash into account using MSC.Adams. The most suitable approach for a fully parameterizable gearbox model, which is desirable to allow for automatic design tools, is used to find an optimal set of parameters with respect to a certain cost function. The gearbox model, with in that sense optimal parameters, is then excited by a nondeterministic wind representation and the contact forces evaluated in time domain. The presented approach is most suitable in terms of being generic and computational efficient.

2 Gear contact model

This section describes two models used to calculate forces acting on gears in contact. The first model is based on a reference CAD gear representation and calculating the contact forces by using MSC.Adams built-in contact description with a certain stiffness and damping. The contact forces depend therefore very much on a proper geometrical surface description. The second model calculates the contact forces by using the gear specific kinematics and applying substitution forces on the respective shaft positions. The advantages and disadvantages are listed as follows:

- CFA (Contact Force Adams) model:
  The contact forces are based on MSC.ADAMS contact functionality between two rigid bodies having a proper surface description. The computation time can therefore be very high, depended on the desired resolution. Modeling and simulation with CAD geometry is in general not modular in the sense that design changes requires having access to an automated gear design tool.
- CFS (Contact Force Subroutine) model:
  Here, the former contact is replaced with substitution forces by using the gear mesh deformation at pitch radius with respect to the angular position and velocity of gears and planet carrier. The contact forces are then calculated and applied at the center of each gear. This approach requires no CAD model and a parametrization of a gearbox model can be achieved. Although, this contact description does not allow the evaluation of contact forces in very detail. The general idea is to get a basic contact formalism which is computational efficient and can therefore be used for a multi-stage gearbox.

2.1 CFA-description

MSC.Adams offers the capability to define contact between geometrical objects based on the following description, see [11]. The normal contact force respectively can be written in MSC.Adams command language.

$$F_{CFA} = k_0 \delta^e + step(\delta, 0, 0, d_{\max}, c_{\max})\dot{\delta} \tag{1}$$

Here, F_{CFA} is a combination of a stiffness related term and a damping related term. The former is calculated with contact stiffness k_0, penetration depth δ and force exponent e which is chosen to be 3/2 based on the Hertzian contact theory for elastic spheres. The damping term is calculated using a Step function along δ starting from 0 damping up to a maximum penetration depth $d_{\max}$ with maximum damping coefficient $c_{\max}$ multiplied with the penetration velocity $\dot{\delta}$.

2.2 CFS-description

The normal contact force used in this approach is based on the Hertz contact relation for elastic spheres with an additional viscous damping term which gives the following relation.

$$F_{CFS} = k_0 \delta_{BL}^{e} + c_0 \left|\delta_{BL}\right| \dot{\delta}_{BL} \tag{2}$$

F_{CFS} has the same stiffness related term as CFA but uses another damping related term. δ_{BL} is the indentation introduced below in subsection 2.3. The contact stiffness and contact damping are denoted as k_0 and c_0 respectively. $|\delta_{BL}|$ assures that there is no damping force when the gears are not in contact. Moreover, it must be taken care that this contact normal force does not change sign during simulation.

2.3 Backlash

In a gear system, backlash is the distance between mating teeth and generally necessary to allow a lubricant film between the gears in contact, to be less sensitive against manufacturing imperfections or an eventual deformation within the system e.g. due to a certain loading or thermal expansion, otherwise the gears could jam. Generally, modeling backlash has a minor role for moderately to heavily loaded gears. Nevertheless, there are circumstances, e.g. load reversals due to wind gusts at low speed, where backlash has a contribution to the peak forces. Motivated by [12] and [13], backlash is modeled by implementing a $tanh$-function by using the following equations:

$$\delta_{BL} = \delta + 1/2(\tilde{g}_1(\delta(t)) - \tilde{g}_2(\delta(t))) \tag{3}$$

$$\begin{aligned} \tilde{g}_1(\delta(t)) &= (\delta - j_t/2)\tanh(\lambda(\delta - j_t/2)) \\ \tilde{g}_2(\delta(t)) &= (\delta + j_t/2)\tanh(\lambda(\delta + j_t/2)) \end{aligned} \tag{4}$$

with δ the linearized distance between the two tooth surfaces and $\tilde{g}_1(f(t))$, $\tilde{g}_2(f(t))$ two tanh-functions whereas j_t being the circumferential backlash value and λ a constant regularization factor controlling the transition between non-contact and full contact. Figure 1 shows eq. 3 for three different λ.

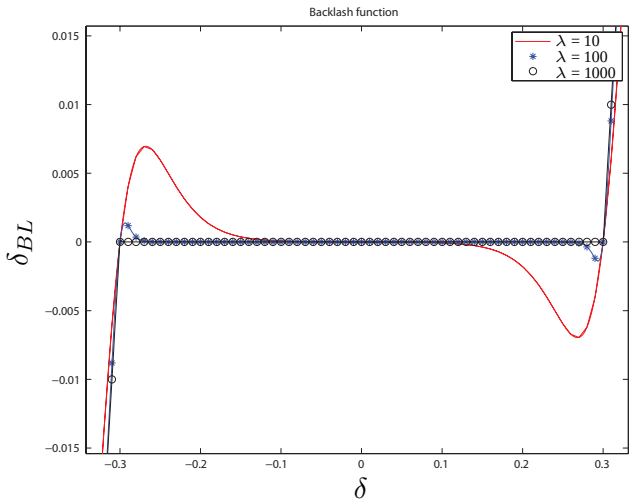

Figure 1: Backlash function for three different regularization factors λ

It should be noted that the regularization factor here plays a double role. The physical interpretation is that in real systems the change from not in contact to full contact having the nominal stiffness value has a certain transition zone due to e.g. lubrication, stiffness distribution related to local deformation or tooth bending. Moreover, there are numerical issues since λ acts as regularization of a ramp-function, thereby improving the convergence of Jacobian iterations.

3 One stage gear

Below, the two former described gear contact models are elaborated in more detail for one stage and compared with each other. The first case is a parallel spur gear with the dimensions from sun and planet, as shown in table 1. In the second case, a planetary gear taking the sun, planet and outer ring is examined. First, the gears are built with Catia using an involute profile and the CAD data then imported into MSC.Adams for applying the CFA. The same gear bodies are hereinafter used to represent mass and inertia properties for the CFS approach. After applying the same input properties, the equivalent contact forces are compared with each other. In both cases backlash is taken into account.

Gear	Sun gear	Planet gear	Outer ring
Module [mm]	10	10	10
Z [-]	22	32	86
Pressure angle α [deg]	20	20	20
Pitch radius $r_{p,i}$ [mm]	110	160	430
Base radius $r_{b,i} = r_{p,i}cos(\alpha)$ [mm]	103.36	150.35	404.06
Linear backlash j_n [mm]	0	0.5	0
Contact ratio ε_i [-]	ε_{SP}= 1.62	ε_{POR}= 5.64	

Table 1: Reference gear definition

3.1 Parallel spur gear

For the spur gear, only the sun gear and one planet gear are taken into account according to table 1 which means the planet is the drive gear whereas the sun is driven in this configuration.

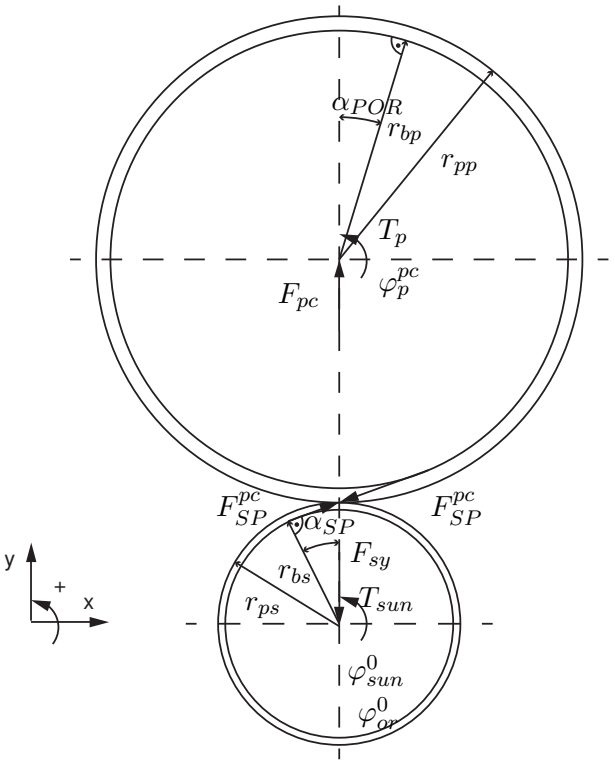

Figure 2: Free body diagram: Parallel spur gear

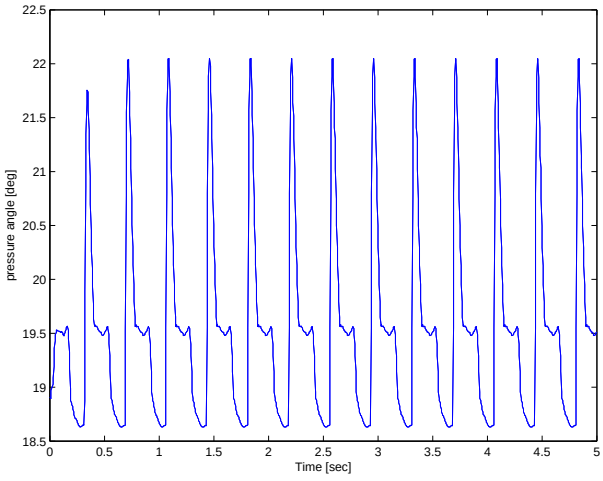

Figure 3: Parallel gear input: ω_{input} = 5 rpm, $T_{c,output}$ = 1 kNm

These contact forces act on the tooth flanks in a constant angle that corresponds to the pressure angle in case

of an involute profile. As shown in figure 3, the instantaneous pressure angle is here not constant because of several reasons e.g. backlash, modeling imperfections of the CAD surface. An increasing backlash leads to deviation from the design pressure angle used for specifying the involute profile. The contact forces are very sensitive in magnitude with respect to the pressure angle. For aligning the two used contact concepts with each other, the mean pressure angle from the CFA model can be computed by taking the $\tan^{-1}$ of the sum of all contact incident forces in x-direction divided by the sum of all contact incident forces in y-direction, taking, shown in figure 3. This approach can just provide an estimate i.e. there are several teeth in contact, the contact area is not necessarily perpendicular to the gear plane and it was further observed that the mean pressure angle is depended on the loading. Due to this reasons, a pressure angle of 20 deg has been used as input for the CFS-description and the deviations of the mean values comparing both approaches are accepted, see tab. 2. The force $F_{SP,CFS}$ is elaborated in more detail in the next chapter 3.2, eq. 8 and can be used here by setting φ_{pc}^{0} = 0. For comparing the two model approaches, the obtained contact force is shown in figure 4. ω_{input} = 5 rpm is the velocity of the drive gear and a counter torque $T_{c,output}$ = 1 kNm is applied on the driven gear. Generally, all inputs in this work are applied as step functions at simulation time t = 0.

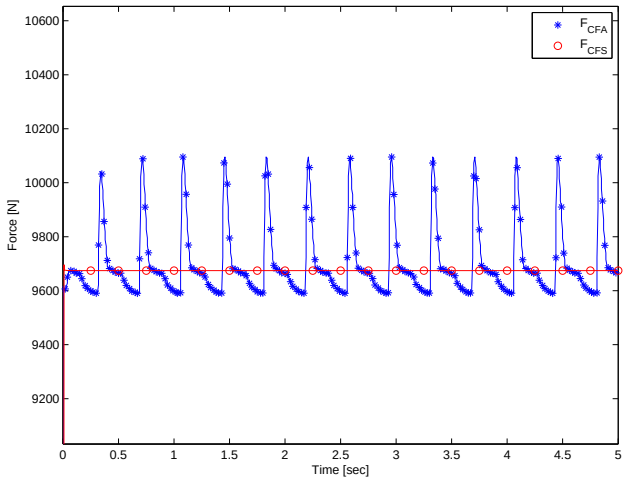

Figure 4: Parallel gear input: ω_{input} = 5 rpm, $T_{c,output}$ = 1 kNm,

Parameter	Mean value
Pressure angle α_{SP}	19.53
$F_{SP,CFA}$ [N]	9.68E3
$F_{SP,CFS}$ [N]	9.67E3

Table 2: Mean values: ω_{input} = 5 rpm, $T_{c,output}$ = 1 kNm

Parameter	Value	Parameter	Value
R [-]	1.5:1	Z_{drive} [-]	32
Penetration depth for CFA [mm]	0.1	Pressure angle α[deg]	20
Module	10	Contact stiffness k_0 [N/mm]	5E4
Linear backlash j_n [mm]	0.5	Contact damping c_0 [Ns/mm]	5E3
Mass drive gear [kg]	24.2	λ [-]	10
Mass driven gear [kg]	11.06	I_{xx} drive gear [kgmm^2]	3.16E5
Width [mm]	40	I_{xx} driven gear [kgmm^2]	7.13E4

Table 3: Parallel stage parameters

According to figure 4 and table 2, for low loads, the mean values of the contact forces are very close to each

other. Table 3 lists all parameters used for this investigation.

3.2 Planetary gear set

For the planetary gear, all gears are specified according to table 1. In this configuration, load is applied on the planet carrier whereas the sun is driven. First, the free body diagram for all components of a planetary gear consisting of a sun gear, one planet gear, outer ring and a planet carrier is presented. The subscript denotes the variable name whereas the superscript denotes the reference coordinates system. Figure 5 shows the used planetary gear configuration and figure 6 the respective free body diagram for one planet.

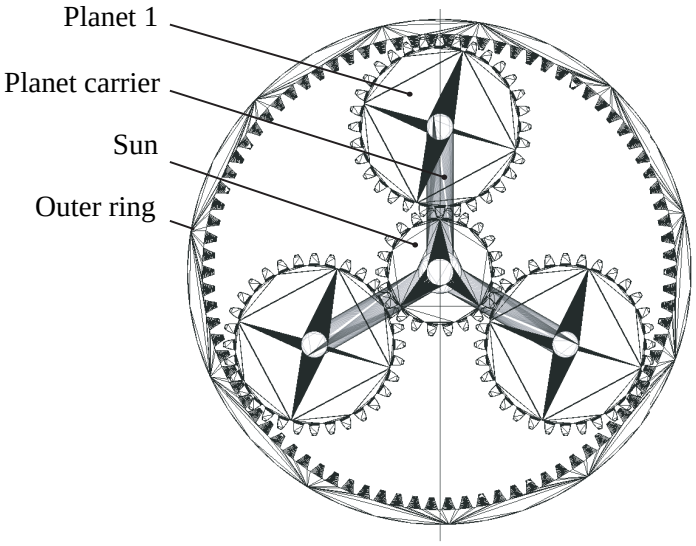

Figure 5: Planetary gear according to table 1

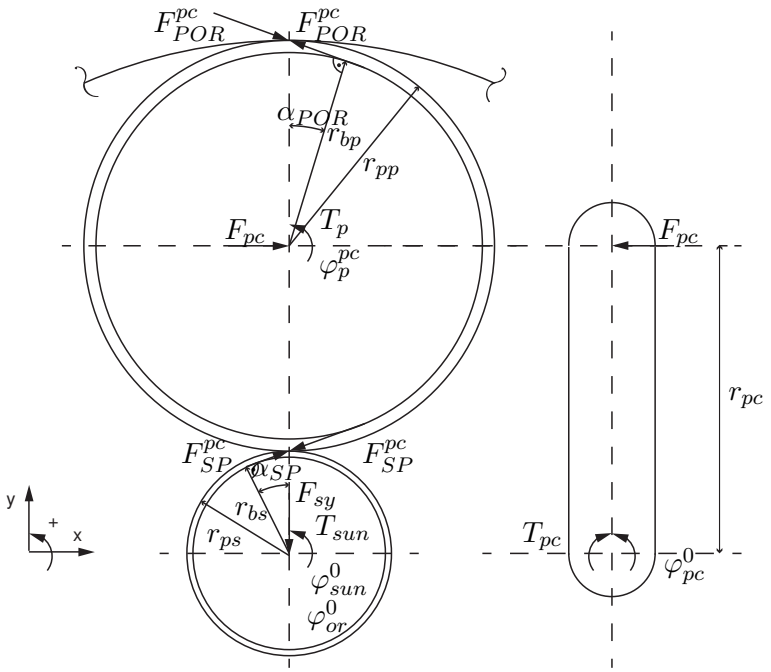

Figure 6: Free body diagram: Planetary gear with one planet

According to figure 6, the equilibrium conditions are derived as follows.

$$\text{Sun} \qquad \begin{cases} \sum M_{Sun,0} = 0 = T_{sun} - F^{pc}_{SP,CFS} r_{bs} \\ \sum F_{Sun,y} = 0 = -F_{sy} + F^{pc}_{SP,CFS} \sin(\alpha_{SP}) \end{cases} \tag{5}$$

$$\text{Planet} \qquad \begin{cases} \sum M_{P,0} = 0 = T_p - F^{pc}_{SP,CFS} r_{bp} + F_{POR,CFS} r_{bp} \\ \sum F_{P,x} = 0 = F_{pc} - F^{pc}_{SP,CFS} \cos(\alpha_{SP}) - F_{POR,CFS} \cos(\alpha_{POR}) \end{cases} \tag{6}$$

$$\text{Planet carrier} \qquad \sum M_{PC,0} = 0 = -T_{pc} + F_{pc} r_{pc} \tag{7}$$

$F^{pc}_{SP,CFS}$ and $F^{pc}_{POR,CFS}$ are the gear contact forces of the sun-planet and the planet-outer ring seen in the body coordinate system of the planet carrier. To enhance readability, the superscript is from now on neglected. F_{SP} and F_{POR} can be found kinematically as described below.
The following paragraph elaborates the contact forces in more detail based on the CFS-description, see 2.2. It is assumed that the angular displacements are small and the following expressions can therefore be expressed in a linearized way.

Based on figure 6, the contact forces can be calculated as follows.

$$F_{SP,CFS} = (\underbrace{\varphi^0_{sun} r_{ps} + \varphi^{pc}_p r_{pp} - \varphi^0_{pc} r_{ps}}_{\delta(.)}) k_0(\delta) + \dot{\delta}(.) c(\delta) \tag{8}$$

$$c(\delta) = |\delta| \, c_0 \tag{9}$$

Here in eq. 8, $F_{SP,CFS}$ is the contact force acting on the tooth flanks of the sun and the planet. The fist term in eq. 8 is the stiffness force. In this term, the angles φ are the rotational positions around the line of rotation in the respective coordinate system for the sun, planet and planet carrier. The distances, denoted as r are the pitch radii of the sun and planet respectively. The indentation $\delta(.)$ is used as input for the backlash function, see eq.3. The second term in eq. 8 is the damping force with damping $c(\delta)$. In this case the damping is chosen to be related to the absolute value of the indentation multiplied by the contact damping according to chapter 2.2, see eq. 9. This ensures that the damping force only applies when the gears are in contact.

$$F_{POR,CFS} = (\underbrace{-\varphi^0_{or}(r_{pc} + r_{pp}) + \varphi^{pc}_p r_{pp} + \varphi^0_{pc}(r_{pc} + r_{pp})}_{\delta(.)}) k_0(\delta) + \dot{\delta}(.) c(\delta) \tag{10}$$

$F_{POR,CFS}$ is the contact force acting on the tooth flanks of the planet and the outer ring with respect to the planet carrier coordinate system. As in eq. 8, the first term describes the stiffness force and the second term the damping force using the same notation for the planet and the planet carrier. One should mention that it is assumed that the outer ring has no angular displacement with respect to the reference frame and therefore $\varphi^0_{or} = 0$ and so the corresponding term vanishes.

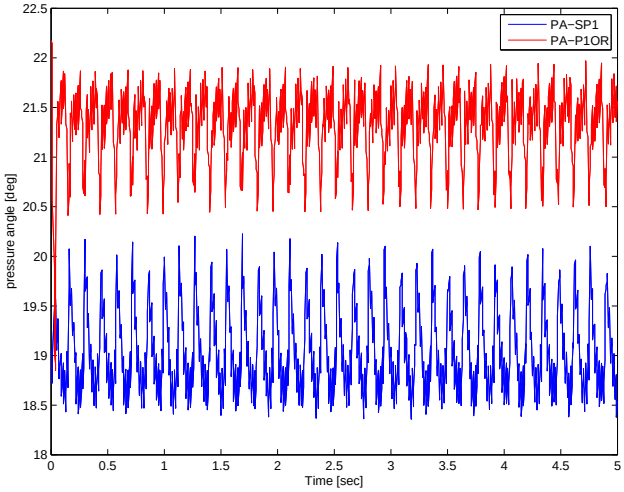

Figure 7: Planetary gear input: ω_{input} = 5 rpm, $T_{c,output}$ = 1 kNm

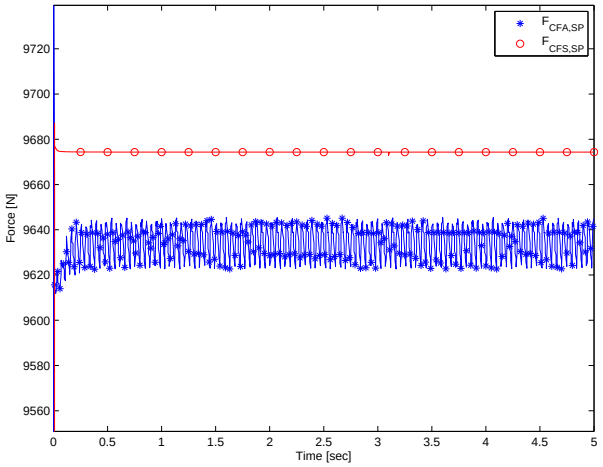

Figure 8: Sum of contact force comparison sun-planet

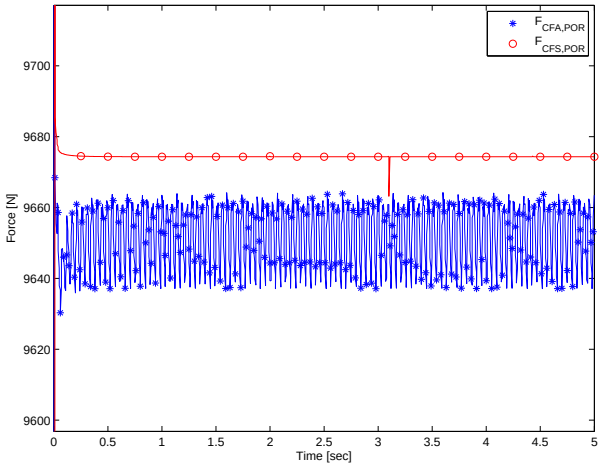

Figure 9: Sum of contact force comparison planet-outer ring

For planetary gears, the contact force is usually not constant at each time instance for each gear pair and therefore the load is not equally distributed to all three planets. Nevertheless, load sharing behavior is out of the scope of this investigation. Therefore, to be able to compare the resulting normal contact forces, the sum of all three sun-planet contact forces and the sum of all three planet-outer ring contact forces has been taken.

Parameter	Mean value
Pressure angle α_{SP1} [deg]	19.05
Pressure angle α_{P1OR} [deg]	21.32
Sum $F_{SP,CFA}$ [N]	9.62E3
Sum $F_{POR,CFA}$ [N]	9.63E3
Sum $F_{SP,CFS}$ [N]	9.66E3
Sum $F_{POR,CFS}$ [N]	9.66E3

Table 4: Mean values: ω_{input} = 5 rpm, $T_{c,output}$ = 1 kNm

The comparison of the contact forces for the planetary gear stage shows, according to figure 8 and figure 9,

a slight deviation of the mean values. It is believed that this offset is again, as mentioned in subsection 3.1, a result from deviating instantaneous pressure angles. The number of teeth in contact varies according to the ratios, ε_{SP} = 1.62 and $\varepsilon_{POR} = 5.64$.

To compare the backlash implementation with respect to the resulting contact forces a sinusoidal varying input velocity ω_{input} =5sin(10t) rpm has been applied with a constant counter torque $T_{c,output}$ = 1 Nm and a contact damping $c_{0,CFS}$ = 50 Ns/mm. The reason for the lower damping only in the CFS case is that a regularization factor λ = 10 leads to a comparable smooth transition from non-contact to contact and therefore to lower peak forces. According to figure 10 and figure 11, both approaches agree very well.

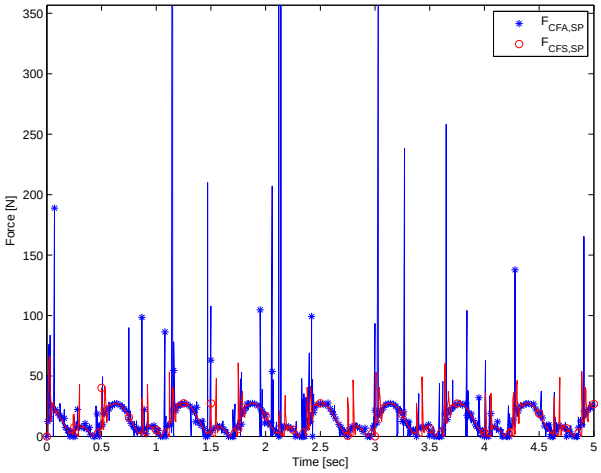

Figure 10: Sum of contact force comparison sun-planet, sinusoidal excitation

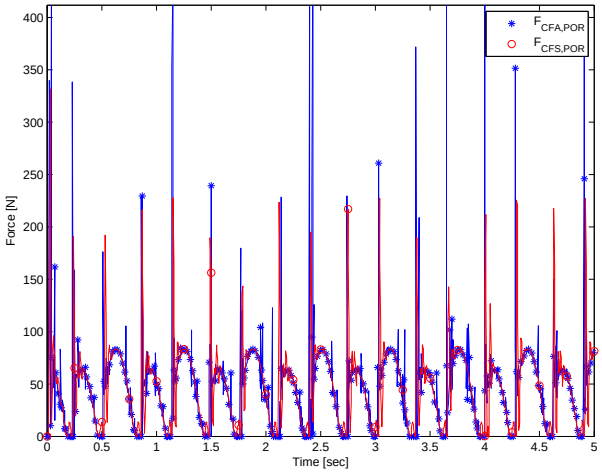

Figure 11: Sum of contact force comparison planet-outer ring, sinusoidal excitation

Parameter	Value	Parameter	Value
R [-]	4.909:1	Z_{sun} [-]	22
Z_{planet} [-]	32	$Z_{outer-ring}$ [-]	86
Pressure angle α[deg]	20	Contact stiffness k_0 [N/mm]	5E4
Module [mm]	10	Contact damping c_0 [Ns/mm]	5E3
Linear backlash j_n [mm]	0.5	λ [-]	10
Mass sun [kg]	11.06	I_{xx} sun [kgmm^2]	7.13E4
Mass planet [kg]	24.2	I_{xx} planet [kgmm^2]	3.16E5
Width [mm]	40		

Table 5: Planetary stage parameters

Table 5 lists all parameters used for this investigation.

4 Multi stage

In this section the CFS model is used to build a fully parameterized multi-stage gear set. This model consists of two planetary stages and one parallel stage with different gear ratios per stage to achieve a desired gearbox ratio of 100:1. Multi-stage gearboxes for wind turbines are usually a combination of planetary stages with a gear ratio of up to 12:1 and parallel stages with a gear ratio up to 5:1. In order to elaborate the complete multi-stage gearbox an analysis in time domain was carried out.

4.1 Analysis in time domain

To investigate the effect of the regularization factor λ together with different stage ratios, a sensitivity analysis was carried out. The complete multi-stage gearbox ratio R_{total} was chosen to be 100:1. The gear ratio of the first planetary stage R_1 was varied linearly from 6:1 to 10:1 in seven steps whereas λ was varied linearly from 10 to 1000 in seven steps. The inputs are ω_{input} = 5 rpm and $T_{c,output}$ = 1 kNm applied on the output gear. The investigated measures are defined by eq. 11 and eq. 12 and computed over the whole time range $0 < t \leq T_{end}$, $T_{end} = 1$ sec.
λ influences the objective function eq. 11 according to figure 12. Increasing λ directly influence the computational time according to figure 13. A desired low objective function $I_{\max,acc}$ can be achieved with a higher gear ratio R_1. The reason for this is due to the underlying assumption that the mass and inertia properties of the second stage are inverse proportional to the gear ratio of the first stage assuming that a lower torque requires less shaft and gear material. It is assumed that the trend on $I_{end,t}$ with respect to R_1, according to figure 13, is that an increase in R_1 leads to increasing accelerations that need to be resolved. For further investigations the set R_1 = 10 and λ = 600 has been chosen.

$$\mathrm{I}_{\max,acc} = \max_t(\dot{\omega}_o), \forall t \in [0, T_{end}] \tag{11}$$

$$\mathrm{I}_{end,t} = T_{cpu} \tag{12}$$

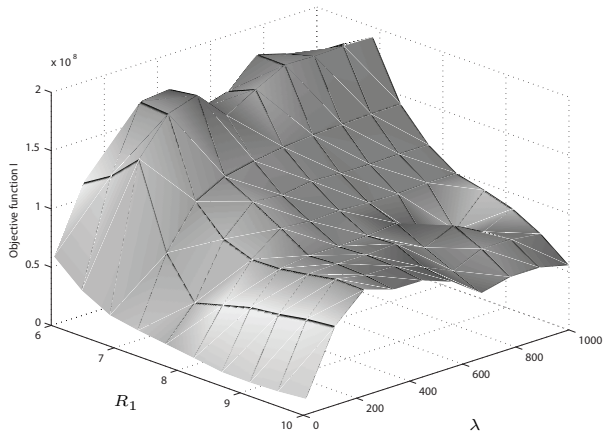

Figure 12: Objective function $I_{\max,acc}$

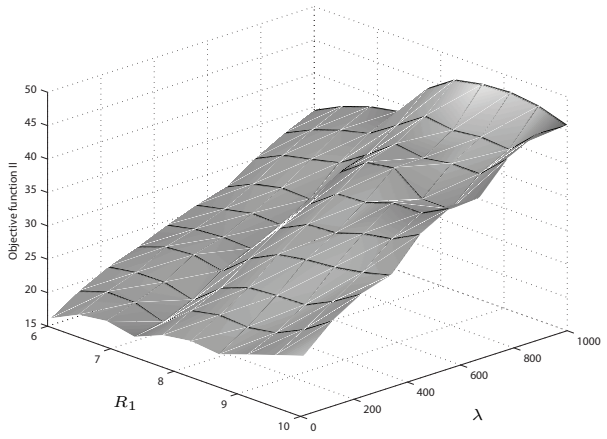

Figure 13: Objective function $I_{end,t}$

As a result of the sensitivity analysis, parameters according to table 6 are chosen for further investigation.

Parameter	Value	Parameter	Value
R_1 [-]	10:1	Z_{sun} stage 1, Z_{sun} stage 2,Z_{drive} [-]	20
R_2 [-]	8:1	Pressure angle α [deg]	20
R_3 [-]	1.25:1	Contact stiffness k_0 [N/mm]	5E5
Module 1st, 2nd a. 3rd stage [mm]	10	Contact damping c_0 [Ns/mm]	5E4
Linear backlash j_n for st, 2nd a. 3rd stage [mm]	0.56	λ [-]	600
Mass sun 1st, 2nd stage [kg]	12.25	I_{xx} sun 1st, 2nd stage [kgmm^2]	6.12E4
Mass planet 1st stage [kg]	196.06	I_{xx} planet 1st stage [kgmm^2]	1.56E7
Mass planet 2nd stage [kg]	11.02	I_{xx} planet 2nd stage [kgmm^2]	4.96E5
Mass drive gear 3rd stage [kg]	12.25	I_{xx} drive gear 3rd stage [kgmm^2]	6.12E4
Mass driven gear 3rd stage [kg]	7.84	I_{xx} driven gear 3rd stage [kgmm^2]	2.50E4
Mass generator rotor [kg]	1531.72	I_{xx} generator rotor [kgmm^2]	1.51E8
Shaft 1 stiffness k_{s1} [Nmm/deg]	1E9	Shaft 1 damping c_{s1} [Nmm/deg]	1E8
Shaft 2 stiffness k_{s2} [Nmm/deg]	1E8	Shaft 2 damping c_{s2} [Nmm/deg]	1E7
Shaft 3 stiffness k_{s3} [Nmm/deg]	1E5	Shaft 3 damping c_{s3} [Nmm/deg]	1E4
Width 1st stage [mm]	50	Width 3rd stage [mm]	50
Width 2nd stage [mm]	5		

Table 6: Multi-stage gearbox parameters after sensitivity analysis

4.2 Analysis of Gearbox implementation in drive train with nondeterministic loading

In this section the gearbox has been subsequently coupled with a rotor mass representing the generator.

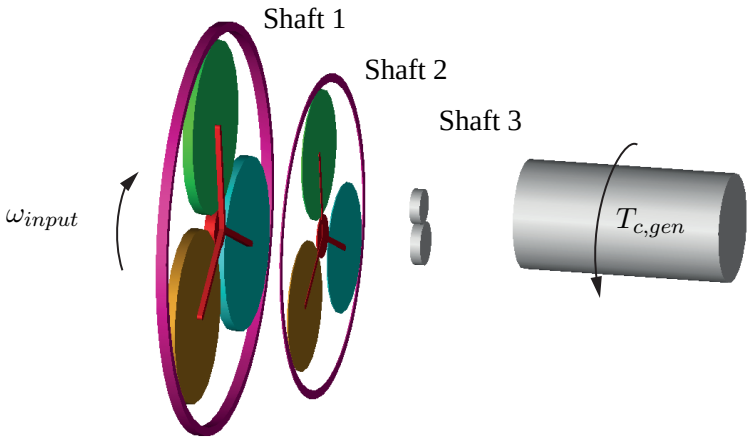

Figure 14: Analysis of Gearbox implementation in drive train

For future research use, the authors seek to investigate how the model performs under loading typical to the wind turbine application. To this end, we consider the low speed shaft rotation speed $\omega(t)$ as prescribed boundary condition. Since $\omega(t)$ ultimately depend on wind speed, it can be viewed as a stochastic process (for common multi-MW wind turbine with sophisticated power electronics), characterized by a mean value ω_0 and a fluctuation described by a power spectrum $S(f)$ (under a reasonable short time, e.g. 10 minutes). Hence, we shall consider the following model for the low speed shaft rotor speed

$$\omega(t) = \omega_0 + \sum_{k=1}^{N} W_k cos(f_k t + \phi_k), \qquad W_k = S(f_k)\Delta f \tag{13}$$

where the phase shifts ϕ_k are independent random variables uniform on $[0, 2\pi]$. The power spectrum $S(f)$ is parameterized as

$$S(f) = ae^{-\frac{a}{\sigma^2}t} \tag{14}$$

σ being the fluctuation intensity and a controlling the slope in frequency domain. The purpose of the investigation is to examine model behavior for parameters ω_0, a, σ. As base values realistic for a multi-MW turbine, $\omega_0 = 16$ rpm, $a = 0.02$ and $\sigma = 0.12$ are chosen. The resulting wind description is shown in figure 15. For analysis, this decryption has been implemented in Matlab environment and run together with MSC.Adams in co-simulation. A time simulation of 60 [sec] was carried out applying the wind description ω_t and a $T_{c,gen}$ = 2.54E7 Nmm at the generator rotor (assuming a 4 MW generator running at 1500 rpm), the output speed of the gearbox can be compared with the output speed of an ideal gearbox. The result is presented by figure 16 where no distinct difference can be noticed.

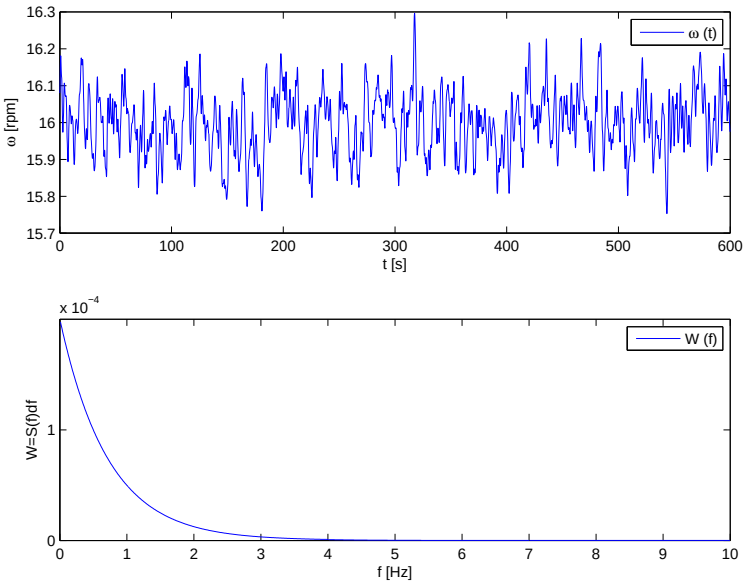

Figure 15: Wind description

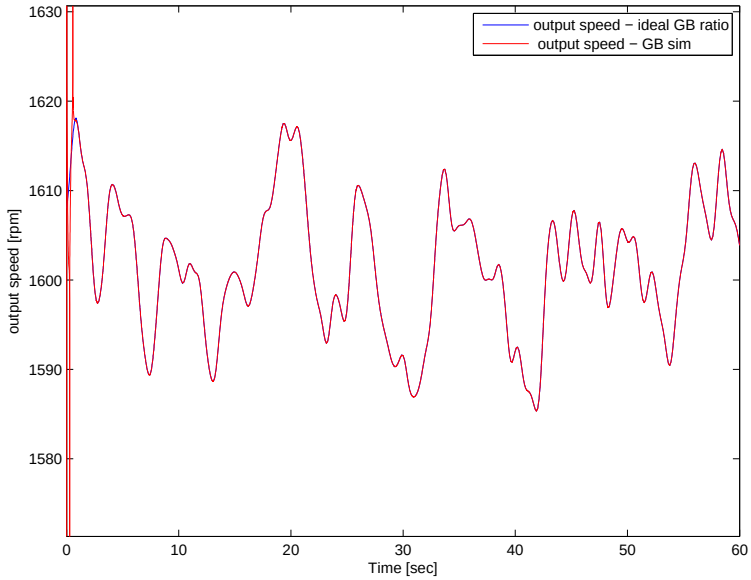

Figure 16: Comparison of output speeds between idealized and simulated gearbox

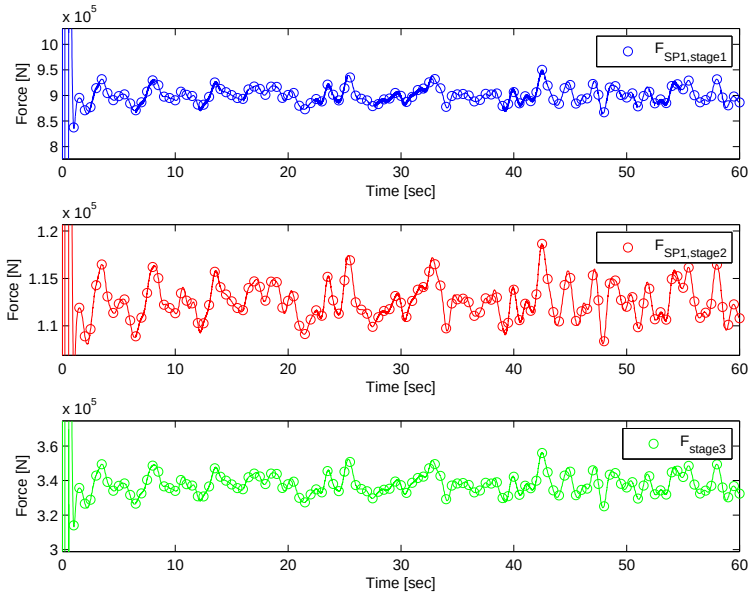

Figure 17: Contact forces of all 3 stages during simulation

Parameter	Mean value	Std value
$F_{SP1,stage1}$ [N]	9.0067e+005	1.5123e+004
$F_{SP1,stage2}$ [N]	1.1261e+005	1.8893e+003
$F_{SP1,stage3}$ [N]	3.3786e+005	5.6738e+003

Table 7: Mean values and standard deviations for nondeterministic load case

Table 7 summarizes the investigation with respect to the contact forces within the interval [5sec,60sec] by showing the mean values and standard deviations. Here, $F_{SP1,stage1}$ has the highest mean value as well as standard deviation.

5 Conclusion

A generic multi-stage gearbox model has been presented. This main advantage has been used to perform a parameter study to find an optimal set of parameters with respect to the used cost function. The model is then further used in the context of a drive train system for a wind turbine by applying a nondeterministic input velocity and a generator representation. Many simplifications are present in this model and some of the parameters were chosen as estimations without having more realistic values. Nevertheless, simplifications during modeling are necessary in order to decrease the computational time. Therefore the results have more qualitative meaning especially because damping has not been considered as a structural damping but applied for numerical reasons. For understanding the complex phenomena occurring in the system, still different hierarchical modeling levels are necessary. Focusing on the contact problem itself requires more sophisticated contact models than the one presented here. The hurdle here is that a combination of tools for macro and micro-scale investigations is necessary which might be difficult to implement. The computational demands of such models can be very high which makes it very time consuming running parameter studies to find optimal structural parameters with respect to e.g. peak forces at certain positions under certain load cases. Several researchers investigated complex gearing phenomena for a wide range of applications, e.g. automotive, maritime or aeronautics. Wind turbine application is different to the former mentioned regarding the nondeterministic excitation due to the nature of the wind, big rotor and generator inertia, exposure to extreme ambient conditions, tower flexibility, shock loads from electrical faults and wind gusts,

large reverse torque during emergency stops, tilting or lateral loads that may be transferred via the gearbox to the bedplate. Ongoing research is looking for the most relevant gearbox phenomena for further development of the presented computational model of a multi-stage gearbox.

Acknowledgement

This work was supported by SWPTC (Swedish Wind Power Technology Centre).

References

[1] Peeters, J., *Simulation of Dynamic Drive Train Loads in a Wind Turbine*, Katholieke Universiteit Leuven, 2006, PhD thesis.

[2] Ribrant, J. and Bertling, L., *Survey of failures in wind power systems with focus on Swedish wind power plants during 1997-2005*, Ieee Power Engineering Society General Meeting (2007), Vols 1-10, 3896-3903.

[3] Link, H., LaCava, W., van Dam, J., McNiff, B., Sheng, S., Wallen, R., McDade, M., Lambert, S., Butterfield, S. and F. Oyague, *Gearbox Reliability Collaborative Project Report: Findings from Phase 1 and Phase 2 Testing*, NREL, National laboratory of the U.S. Department of Energy, 2011.

[4] Ozguven, H. N. and Houser, D. R., *Mathematical-Models Used in Gear Dynamics - a Review*, Journal of Sound and Vibration (1988), 121 (3), 383-411.

[5] Wang, Jianjun and Li, Runfang and Peng, Xianghe, *Survey of nonlinear vibration of gear transmission systems*, Applied Mechanics Reviews (2003), 56 (3), 309-329.

[6] A.Palermo, D. Mundo, A.S. Lentini, R. Hadjit, P. Mas, W. Desmet, *Gear noise evaluation through multibody TE-based simulations*, Proceedings of the "ISMA 2010", Belgium.

[7] Peeters, J. L. M. and Vandepitte, D. and Sas, P, *Analysis of internal drive train dynamics in a wind turbine*, Wind Energy (2006), 9, 1-2, 141-161.

[8] Kim, Woohyung and Yoo, Hong Hee and Chung, Jintai, *Dynamic analysis for a pair of spur gears with translational motion due to bearing deformation*, Journal of Sound and Vibration (2010), 329 (21), 4409-4421.

[9] Todorov, M. and Dobrev, I. and Massouh, F., *Analysis of Torsional Oscillation of the Drive Train in Horizontal-Axis Wind Turbine*, 8th International Symposium on Advanced Electromechanical Motion Systems (Electromotion 2009), 56-62.

[10] Todorov, M., *Modal Properties of Drive Train in Horizontal-Axis Wind Turbine*, Proceedings of International Conference On Innovations, Recent Trends And Challenges In Mechatronics, Mechanical Engineering And New High-Tech Products Development – MECAHITECH (2011), vol. 3.

[11] MSC (2011), *About Adams/Solver*, MSC.

[12] Kim, T. C., T. E. Rook, et al. (2003), *Effect of smoothening functions on the frequency response of an oscillator with clearance non-linearity*, Journal of Sound and Vibration 263(3): 665-678.

[13] Walha, L. and Fakhfakh, T. and Haddar, M., *Backlash effect on dynamic analysis of a two-stage spur gear system*, Journal of Failure Analysis and Prevention (2006), 6 (3): 60-68.